



Binding of α -lipoic acid to human serum albumin: spectroscopic and molecular modeling studies

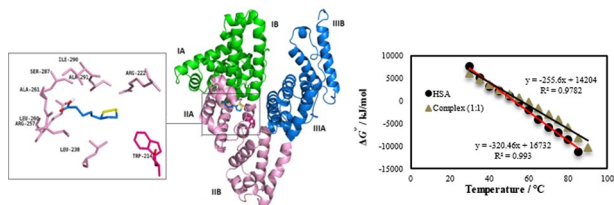
Fatemeh Toosi-Moghadam¹ · Mehdi Khoobi² · Ali Akbar Saboury¹ · Zahra Allahdad¹ · Anahita Khammari^{1,3} · Arefeh Seyedarabi¹ · Leila Karami⁴ · Atiyeh Ghasemi¹ · Luciano Saso⁵

Received: 10 August 2021 / Accepted: 4 October 2021 / Published online: 19 October 2021
© Springer-Verlag GmbH Austria, part of Springer Nature 2021

Abstract

α -Lipoic acid as an antioxidant is used in the treatment of many diseases, such as diabetes, cardiovascular diseases, cancer, and AIDS. The objective of this study was to investigate the capability of human serum albumin (HSA) as a potential carrier for α -lipoic acid (α -LA). Molecular interactions between HSA and α -LA were monitored via fluorescence and circular dichroism spectroscopies as well as molecular docking and molecular dynamics simulations studies. The results revealed that α -LA binds to HSA with binding stoichiometry of 1:1 through hydrogen bonding and van der Waals interactions. The overall binding affinity was estimated to be of the order 10^5 M^{-1} . α -LA induced partial folding in the tertiary structure and subtle alterations in the secondary structure of HSA, which was accompanied by increased thermal stability. The results also demonstrated that the complex formation between α -LA and HSA enhanced photostability under UV irradiation. The improved antioxidant activity of α -LA in electron donation was amongst the positive influences observed through the association of α -LA with HSA. Thus, their complexes can successfully be employed in the food and pharmaceutical industries.

Graphic abstract



Keywords Fluorescence spectroscopy · Circular dichroism · Photostability · Molecular simulation · α -Lipoic acid

✉ Ali Akbar Saboury
saboury@ut.ac.ir

- 1 Institute of Biochemistry and Biophysics, University of Tehran, Tehran, Iran
- 2 Biomaterials Group, The Institute of Pharmaceutical Sciences (TIPS), Tehran University of Medical Sciences, 1417614411 Tehran, Iran
- 3 Department of Biophysics, School of Biological Sciences, Tarbiat Modares University, Tehran, Iran
- 4 Department of Cell and Molecular Biology, Faculty of Biological Science, Kharazmi University, Tehran, Iran
- 5 Department of Physiology and Pharmacology “Vittorio Erspamer”, Sapienza University of Rome, Rome, Italy

Introduction

α -Lipoic acid (1,2-dithiolane-3-pentanoic acid; α -LA) is a medium chain (C_8) fatty acid with a cyclic disulfide bond served as a cofactor in the mitochondrial energy metabolism in prokaryotic and eukaryotic cells [1, 2]. It can also exist in the reduced form known as dihydrolipoic acid (DHLA), which is able to interact with reactive oxygen species (ROS) [3]. Its therapeutic applications to prevent various diseases associated with oxidative stress due to having strong antioxidant activity are rapidly growing [4, 5]. α -LA has some health benefits, such as improving carbohydrate metabolism and renal function, lowering blood pressure, and

normalizing associated biochemical and histopathological changes. Thus, α -LA is utilized as a dietary supplement in the food industry and has been suggested for its application as an antioxidant supplement [6, 7]. In addition, the ability of α -LA in delaying the adverse effects resulting from aging has also promoted the application of α -LA as a functional cosmeceutical agent [8–11].

Nevertheless, α -LA utilization in various industries has been restricted due to its poor water solubility and its instability against oxidation, UV irradiation, and high temperatures [12, 13]. The latter, especially at temperatures above its melting range (321–323 K) is accompanied by polymerization of the distorted five-membered ring of dithiolane. The polymerization and oxidative degradation of α -LA result in reduction of its bioactivity and loss of flavor. The high elimination rate of α -LA, with a biological half-life of less than 30 min [14], suppresses its widespread use in food and clinical industries. Thus, a strategy should be used to enhance its solubility, stability, and bioavailability.

Various carriers, such as chitosan [15], cyclodextrins [16–18], nanostructured lipids [19], and high amylose starches, whether native or substituted with octenylsuccinyl groups [20], have already been employed to eliminate the shortcomings of α -LA. To the best of our knowledge, there are no reports, where proteins have been used as delivery systems for α -LA, although binding behavior of α -LA to bovine serum albumin has been investigated in a study by Suji et al. [21].

Biomacromolecules such as proteins constitute an integral part of the human diet and are characterized by numerous ligand-binding sites, which can serve as ideal carriers for free α -LA. Human serum albumin (HSA) is the most abundant protein in the blood plasma showing an extraordinary ligand-binding capacity. Numerous endogenous and exogenous compounds are transported by HSA and as such can be used as a natural and reliable drug carrier. Additionally, HSA is non-toxic, non-antigenic, and more importantly an endogenous protein. The stability of HSA within the pH range of 4–9 and temperatures up to 333 K for 10 h [22] has encouraged many researchers to exploit this valuable protein as a carrier for many food ingredients.

HSA is a single-chain polypeptide of 585 amino acids, folded into three homologous domains (I, II, and III), each composed of two sub-domains (A and B) with common structural elements [23]. This acidic protein has a molar mass of about 66.5 kDa. HSA has no β -sheet structure and is predominantly composed of α -helix content, constituting of up to about 67% of the total structure [22–24]. The tertiary structure of HSA is stabilized by 17 disulfide bridges, which are not exposed to the solvent at neutral pH. On the other hand, observable changes in the shape and size of the protein can occur under different external conditions [25]. According to crystal-state X-ray high resolution HSA structures

published in different literatures, there are two main versatile ligand-binding sites with high affinity for diverse molecules on HSA known as ‘Sudlow’s sites’ (I and II) which are located in sub-domains IIA and IIIA. Four metal-binding sites of different structures, metal ion specificities, and binding affinities have been identified for HSA. In addition, fatty acids adopt 9 binding sites on HSA structure showing different affinities two of which overlap with Sudlow’s sites. Despite the substantial diversity of high-, medium-, and low-affinity ligands, only two well-defined and distant spatial conformations of HSA have so far been documented: one for the defatted HSA and one for fatted HSA [26]. Also, in some studies, *in silico* methods were applied to obtain more details about the binding mode of small molecule to proteins, at the atomic level [27, 28].

The aim of this work was to investigate the interaction between HSA and α -LA using steady-state fluorescence and circular dichroism spectroscopies. Molecular docking and molecular dynamics simulations were also performed to obtain the molecular details of the binding between α -LA and HSA. Finally, the stability and antioxidant activity of the resulting complex were monitored as a new nutraceutical tool.

Results and discussion

Binding analysis using fluorescence spectroscopy

The intrinsic fluorescence of HSA mainly originates from a single tryptophan residue, Trp 214 [29]. In this study, the interaction of HSA with α -LA was investigated through fluorescence quenching of the protein as an analytical tool. The HSA fluorescence spectra were recorded in the presence of different amounts of α -LA. As shown in Fig. 1a, the fluorescence intensity of HSA at different temperatures was gradually quenched with elevating concentrations of α -LA ranging from 0 to 19.6 μ M. Generally, two different mechanisms including static and dynamic or combined are responsible for fluorescence quenching. Dynamic type refers to a process in which the fluorophore and the quencher encounter during the lifespan of the excited state of fluorophore [30]. To elucidate the exact quenching mechanism, Stern–Volmer model was fitted onto the fluorescence data of Figs. 1a, 1Sa, and 1Sb using Eq. (1) [30], as follows:

$$\frac{F_0}{F} = 1 + K_{SV}[\alpha\text{-LA}] = 1 + k_q\tau_0[\alpha\text{-LA}], \quad (1)$$

where F_0 and F are fluorescence intensities in the absence and presence of quencher (α -LA), respectively. k_q is the quenching rate constant of the biological macromolecule, K_{SV} denotes the Stern–Volmer quenching constant and

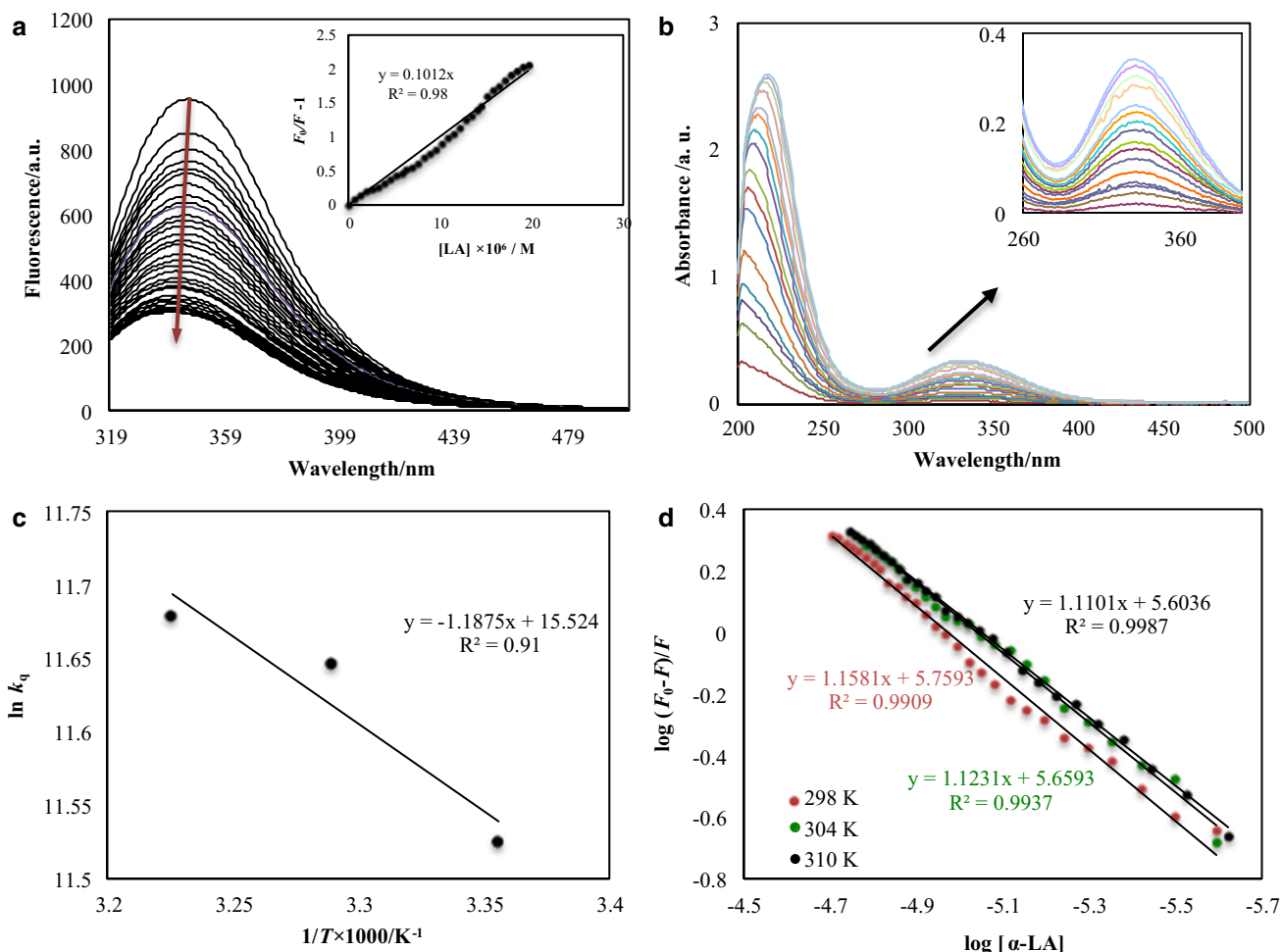


Fig. 1 Fluorescence emission spectra of HSA in 10 mM phosphate buffer has pH 7.4 at 25 °C in the presence of different molar ratios of α -LA to HSA (from 0 to 12.27 μ M) (λ_{ex} = 295 nm). Insets: the Stern–Volmer plot (a). UV/Vis absorption spectra of 3 μ M HSA in the presence of different concentration of α -LA (0–3.5 mM) in 10 mM pH

7.4 phosphate buffer at 25 °C. The maximum peaked at about 330 nm is characteristic for α -LA (b). The plot of $\log [(F_0-F)/F]$ as a function of $\log [\alpha\text{-LA}]$ for the binding of α -LA to HSA at different temperatures (c). The Arrhenius plot of α -LA and HSA system (d)

τ_0 represents the average fluorescence lifetime of the biomolecule in the absence of α -LA equaling to 10^{-8} s. A k_q value higher than $2 \times 10^{10} \text{ M}^{-1} \text{ s}^{-1}$ implies that the resulting quenching is caused by ground-state complex formation [31, 32]. A k_q value around $2 \times 10^{10} \text{ M}^{-1} \text{ s}^{-1}$ indicates collisional quenching [30]. A good linear relationship was observed for Stern–Volmer plots at three temperatures of 298, 304, and 310 K according to the inset of Fig. 1a,

1Sa, and 1Sb. The K_{SV} values obtained from Eq. (4) were 1.01×10^5 , 1.14×10^5 , and $1.18 \times 10^5 \text{ M}^{-1}$ at 298, 304, and 310 K, respectively (Table 1). Accordingly, k_q values corresponding to three temperatures were 1.01×10^{13} , 1.14×10^{13} and $1.18 \times 10^{13} \text{ M}^{-1} \text{ s}^{-1}$, respectively, being nearly 1000-fold greater than the maximum scattering collision quenching constant.

Table 1 Effect of temperature on quenching constants, binding and thermodynamic parameters of HSA in the presence of α -LA

Method	T/K	$K_{sv}/10^5 \text{ M}^{-1}$	$K_a/10^5 \text{ M}^{-1}$	n	$\Delta G^\circ/\text{kJ mol}^{-1}$	$\Delta H^\circ/\text{kJ mol}^{-1}$	$\Delta S^\circ/\text{J mol}^{-1} \text{ K}^{-1}$
Fluorescence	298	1.01 ± 0.35	5.31 ± 0.23	1.15 ± 0.07	-32.69 ± 1.01	-36.209 ± 1.96	-11.82 ± 0.93
	304	1.14 ± 0.52	4.11 ± 0.19	1.11 ± 0.06	-32.62 ± 1.01		
	310	1.18 ± 0.29	3.01 ± 0.11	1.08 ± 0.04	-32.54 ± 1.01		
Calorimetry	–	–	3.19 ± 0.65	0.86 ± 0.025	–	-40.12 ± 1.82	-29.30 ± 0.50

The UV–Vis absorption spectra of HSA in the presence of α -LA (Fig. 1b) exhibited a considerable red shift at a wavelength of 203 nm for HSA, together with a hyperchromic shift with elevating α -LA concentration. Based on these results and UV–Vis absorption spectra of HSA in the presence of α -LA, quenching between β -C and HSA is probably due to static quenching through complex formation. Nevertheless, there is an adverse temperature dependence in a static quenching process. For a more thorough investigation, we used Arrhenius model to predict this anomaly. According to Arrhenius model, the bimolecular rate constant of the quenching process (k_q) should significantly depend on temperature. At higher temperatures, the rate constant should also be higher. Based on this theory, the activation energy of the process (E_a) is also related to the rate constant and the temperature as [33]

$$\ln k_q = \ln A - \frac{E_a}{RT}, \quad (2)$$

where A denotes the pre-exponential factor. Activation energy of the reaction was estimated to be 9.87 kJ/mol (Fig. 1c), which is greater than that of many other reactions between organic compounds and serum albumin [34, 35]. This confirms the remarkable impact of temperature on the fluorescence quenching, strongly supporting static quenching mechanism.

When small molecules bind independently to a set of equivalent sites on a macromolecule with a binding constant K_a , the binding stoichiometry, n , can be estimated from the double logarithm regression curve of $\log [(F_0 - F)/F]$ vs. $\log [\alpha\text{-LA}]$ according to Eq. (3) [30], as follows:

$$\text{Log}[(F_0 - F)/F] = \log K_a + n \log [\alpha\text{-LA}]. \quad (3)$$

Based on this, the parameters of K_a and n were estimated from Fig. 1d and tabulated in Table 1. As seen, α -LA exhibited

a binding affinity towards HSA of the order of 10^5 M^{-1} . Elevation of the temperature from 298 to 310 K reduced the binding constant implying that the complex is less stable at a higher temperature. The values of n , which were estimated to be up to 1, are indicative of a single binding site on HSA for α -LA.

Binding stoichiometry

To determine the stoichiometry of the resulting complex, the Job's method was applied to plot a parameter proportional to the complex concentration vs. molar fraction of protein as displayed in Fig. 2a. The maximum of Job's plot occurred at a molar ratio of 0.5 ($\frac{[\text{HSA}]}{[\alpha\text{-LA}]}$) indicating that one HSA molecule would bind to one α -LA molecule, which is in accordance with the number of binding sites calculated by the Eq. (3) [36, 37].

Binding mode

The interaction forces, which associate small molecules with proteins, include hydrogen bondings, van der Waals forces, as well as hydrophobic and electrostatic interactions. The sign and magnitude of thermodynamic parameters including standard changes of enthalpy (ΔH°) and entropy (ΔS°) of the complex formation provide information about forces contributing to these associations [38, 39]. When $\Delta H^\circ > 0$ and $\Delta S^\circ > 0$, there are hydrophobic interactions; when $\Delta H^\circ < 0$ and $\Delta S^\circ < 0$, there are van der Waals forces and hydrogen bonds; when $\Delta H^\circ < 0$ and $\Delta S^\circ > 0$, there are electrostatic forces. Both thermodynamic parameters can be calculated based on the van't Hoff equation [40], as follows:

$$\ln K_a = -\frac{\Delta H^\circ}{RT} + \frac{\Delta S^\circ}{R}, \quad (4)$$

where R is the gas constant ($8.314 \text{ J mol}^{-1} \text{ K}^{-1}$) and the temperatures used were 298, 304, and 310 K. The van't Hoff plot for three temperatures is depicted in Fig. 2b. The free

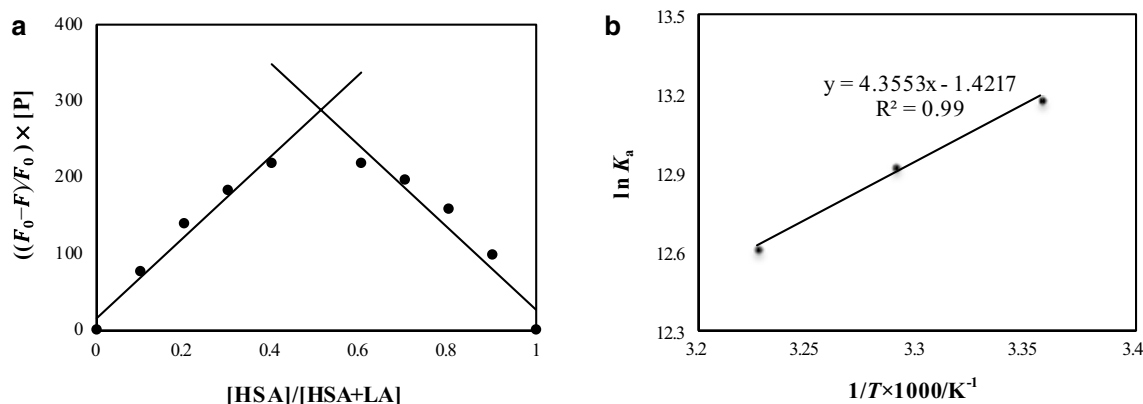


Fig. 2 Job's plot of α -LA bound to HSA in phosphate buffer (10 mM, pH 7.4) at 25 °C, $[\text{HSA} + \alpha\text{-LA}] = 3 \mu\text{M}$ (a). The van't Hoff plot of $\ln K_a$ as a function of $1/T$ for the binding of α -LA to HSA at pH 7.4 (b)

energy change for the complexation can be estimated using the subsequent equation [41], as follows:

$$\Delta G^\circ = \Delta H^\circ - T\Delta S^\circ. \quad (5)$$

Thermodynamic parameters are presented in Table 1. The values of $-36.21 \text{ kJ mol}^{-1}$ and $-11.82 \text{ J mol}^{-1} \text{ K}^{-1}$ for ΔH° and ΔS° , respectively, were calculated from Eq. (7). The negative values of ΔH° , ΔS° , and ΔG° suggest that the interaction is spontaneous and the hydrogen bonding and van der Waals interactions are the main driving forces in the α -LA binding to HSA. Further, the binding process is mainly enthalpy-driven and exothermic [39, 42, 43].

Molecular docking and molecular dynamics simulation

To complement the experimental results, α -LA was docked onto the HSA molecule to determine the possible binding sites. Initially, a global/blind docking was done through building a grid volume covering the entire surface of the protein (using a grid spacing with default value of 1 Å), since it was not known, where on HSA the α -LA molecule would bind to. Higher binding affinity was chosen as the criteria to select the best preferential binding site of α -LA in HSA. Accordingly, the first docking pose (Fig. 3) was

selected (near to Trp). These data are in good agreement with experimental data (fluorescence spectroscopy).

To obtain details about the key residues and dominant interactions, a local docking was performed, where the grid box was centered approximately at the center of the above-mentioned region (near to Trp). Finally, the HSA- α -LA complex with the lowest binding energy was employed as initial structure for molecular dynamics (MD) simulation study. As indicated in Fig. 3, in HSA- α -LA system, α -LA was positioned in a hydrophobic pocket in the region between IIA, IIB, and IIIA sub-domains.

Two MD simulations were carried out for free HSA and α -LA-HSA complex. To investigate the stability of the simulations, the time evolution of root mean square deviations (RMSD) of C α atoms of the protein relative to the initial structures was calculated (Fig. 4a). This figure shows that the RMSD values were in equilibrium in both systems, suggesting that all systems were stable. The RMSD values for HSA was reduced upon binding to α -LA. The RMSD average values (0.30 and 0.26 nm for free HSA and α -LA-HSA complex, respectively) confirmed that the presence of α -LA near to Trp in HSA caused the stability of HSA.

The radius of gyration (R_g), as a measure of system compactness and the solvent accessible surface area (SASA), was computed as a parameter to estimate the exposure of amino acids to the solvent. As shown in Fig. 4b, c, the presence of

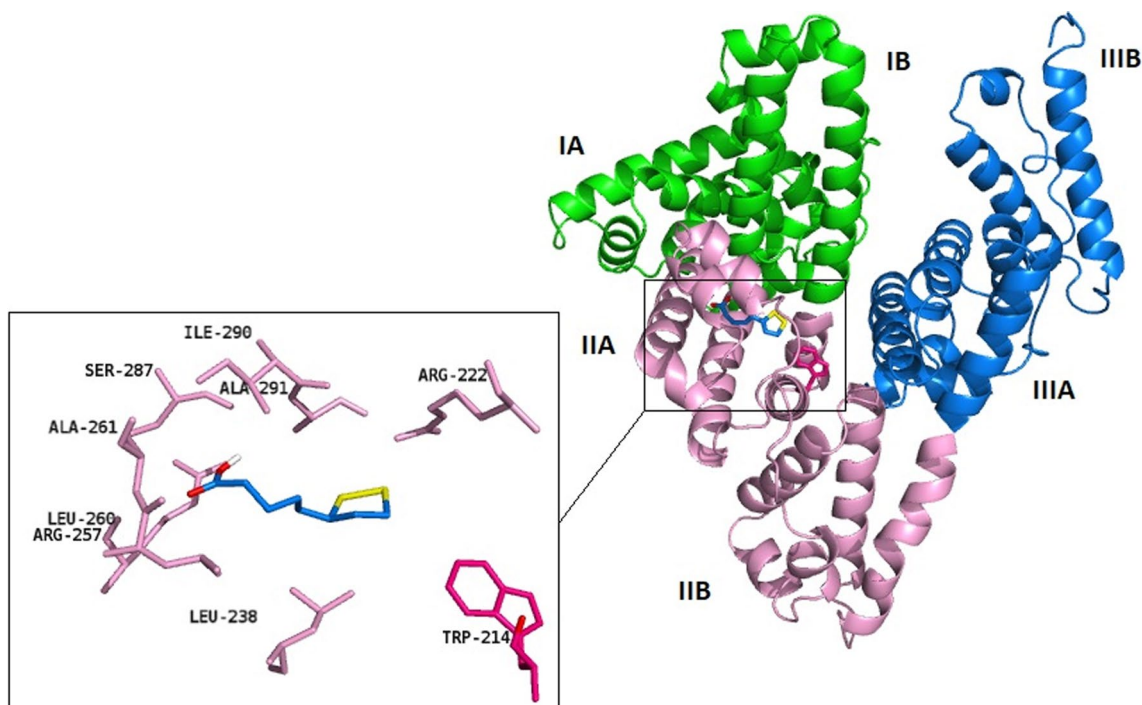


Fig. 3 Location of α -LA molecule in the active site of HSA, after the molecular docking. The α -LA molecule, Trp residue (color in hot pink) and HSA are shown in stick and cartoon representations, respectively. HSA domains of I, II, and III are illustrated in green,

pink, and blue, respectively. Besides, close up view of α -LA molecule binding pose with HSA is specified with the black rectangle. The interacting residues are shown in stick pink representation) (color figure online)

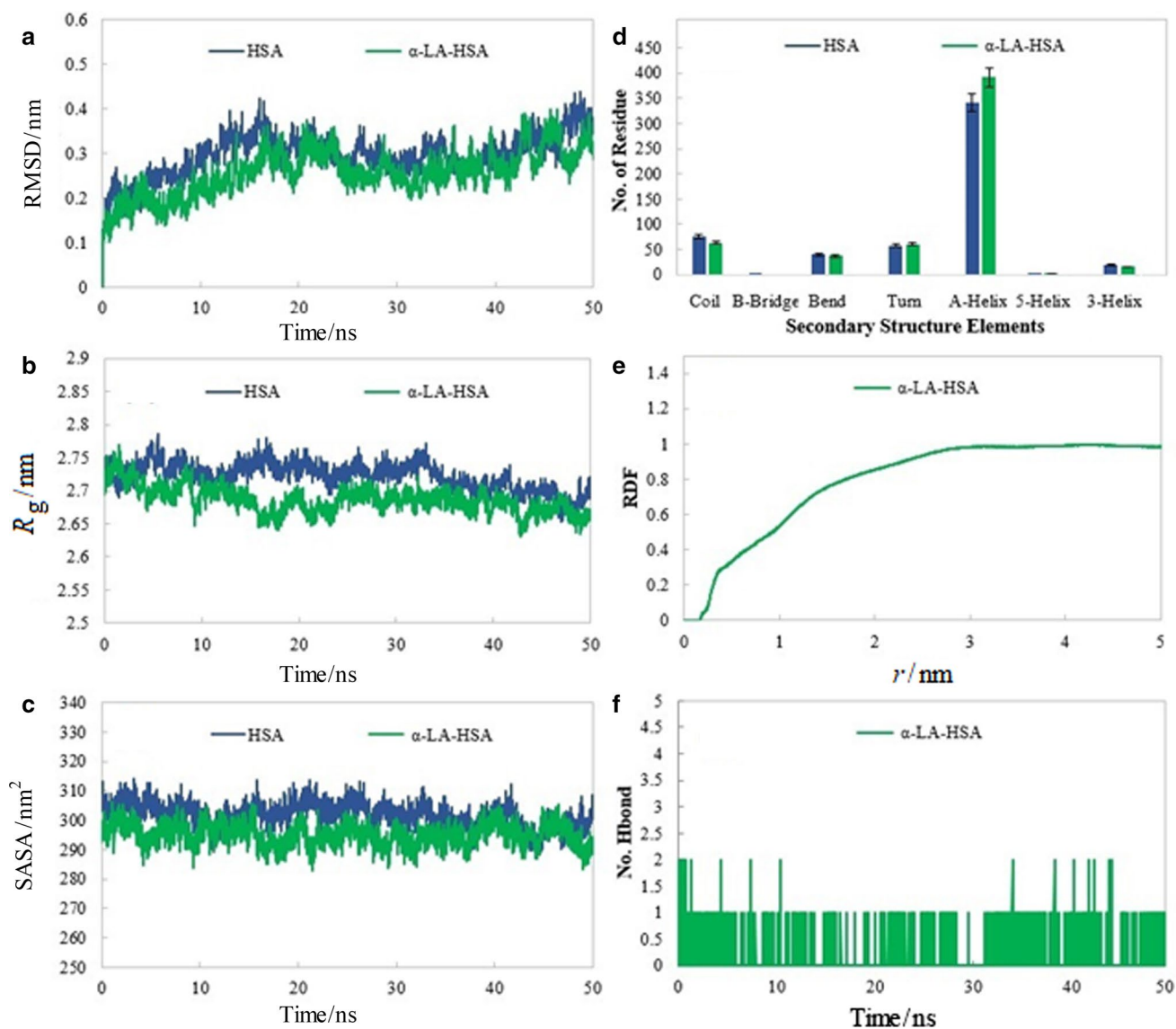


Fig. 4 Analysis of MD simulations results. Root mean square deviation (RMSD) of HSA C α atoms relative to the initial structure (a). Radius of gyration (R_g) of HSA (b). Solvent accessible surface area

(SASA) of HSA (c). Number of residues adopting secondary structural elements. e Radial distribution function (RDF) for water molecules relative to α -LA molecule. f Number of hydrogen bonds (d)

α -LA near to Trp in HSA resulted in a more compact system and less accessible surface area to water solvent, indicating the stabilization role of α -LA in HSA. The R_g and SASA average values confirmed this point well (R_g : 2.72, 2.68, SASA: 301, 295 for free HSA, and α -LA-HSA complex, respectively). Generally, α -LA binding to HSA would lead to more folding in HSA. These results concur with the blue shift observed in the HSA fluorescence spectrum during titration with α -LA.

To survey the structural changes resulting from α -LA binding to HSA, the secondary structure was analyzed using the DSSP program [44]. To this aim, the average number of residues adopting secondary structural elements

was calculated for all simulated systems. As depicted in Fig. 4d, α -LA binding to HSA resulted in a rise in the number of residues participating in the α -helix conformation and a reduction in the number of residues participating in the random coil conformation. These data are in good accordance with CD data. Changes in the number of other secondary structural elements (bend, turn, and 3_{10} -helix) were negligible.

Radial distribution function (RDF) of the water molecules relative to α -LA molecule was calculated for the α -LA-HSA complex. As shown in Fig. 4e, the probability of the placement of water molecules around α -LA molecule in α -LA-HSA complex is low, which can be attributed to the

fact that in the α -LA–HSA system, α -LA is located in the hydrophobic pocket of HSA.

In this study, hydrogen bonds and hydrophobic interactions were assessed to achieve more accurate data about residues contributing to interactions with α -LA. The hydrogen bonding analysis was performed with the number of hydrogen bonds in the α -LA–HSA complex shown in Fig. 4f. The placement of α -LA in hydrophobic pocket of HSA and the orientation of α -LA resulted in a low number of hydrogen bonds. This is also due to the low number of hydrogen bond donor/acceptor in the chemical structure of α -LA. To evaluate the hydrophobic interactions, the LIGPLOT software [45] was used. A number of snapshots (PDB files containing HSA– α -LA complex) were taken during simulation and were applied as input files for LIGPLOT software.

The residues involved in the hydrophobic interactions and hydrogen bonding between α -LA and HSA during the simulations are shown in Fig. 5. As can be seen, both of these interactions are important to establish stability in α -LA–HSA complex. Nevertheless, keep in mind that the number of hydrogen bonds was low for two reasons: (1) the low number of hydrogen bond donor/acceptor in the chemical structure of α -LA (only one carboxyl group) and (2) the placement of α -LA in hydrophobic pocket of HSA and its orientation. These results are well in line with the experimental data [14–16].

Site-specific competitive binding

Note that the fluorescence intensity of warfarin, with a well-defined binding location on HSA, increases when it is transferred from a polar and aqueous environment to a hydrophobic binding site on HSA. The binding of warfarin to HSA has been studied extensively and their

complex has been characterized using X-ray crystallography, clearly confirming the location of the drug binding in the subdomain IIA cavity [46]. Thus, warfarin was used as a specific site marker for the subdomain IIA cavity, which is the preferential binding site for α -LA and can compete with warfarin and change its fluorescence signal. The binding constant of HSA in combination with warfarin was estimated to be $3.47 \times 10^5 \text{ M}^{-1}$ (Fig. 2S), which is in agreement with the values already obtained through fluorescence studies [47].

α -LA accommodation within a hydrophobic site on HSA was monitored through the peak corresponding to α -LA at 590 nm. As can be seen in Fig. 3S, the fluorescence intensity respective to the peak of α -LA bound to HSA is considerable compared to free α -LA at the final concentration of titration, indicating α -LA confinement in a hydrophobic environment. To find the exact ligand-binding location, a site-competitive displacement experiment was carried out between α -LA and warfarin. Through gradual addition of warfarin to the HSA solution, the dell of peak intensity of HSA coincided with a clear red shift due to warfarin accommodation in its own binding site and the formation of the HSA–warfarin complex (Fig. 6a). Next, by halting the addition of warfarin to the protein solution and subsequently adding α -LA to the binary system of HSA–warfarin, the peak intensity of HSA attached to warfarin decreased without any observable shift (Fig. 6a). This implies that the second quenching is the result of α -LA association with HSA in a site located in subdomain IIA. The reduction of peak intensity corresponding to HSA–warfarin complex revealed at 380 nm (by exciting at 330 nm) with gradual addition of α -LA confirmed the displacement of warfarin by α -LA in subdomain II A (Sudlow site I) (Fig. 6b).

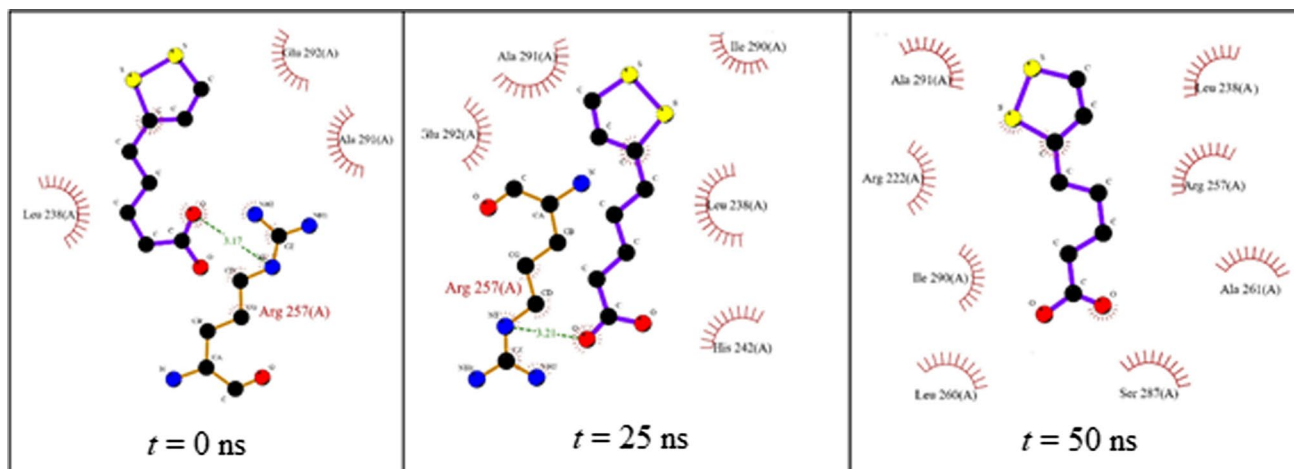


Fig. 5 Schematic diagram of protein–ligand (HSA– α -LA) interactions generated by LIGPLOT. Hydrogen bonds are green dashed lines. Hydrophobic contacts with the ligand are represented by red semi-circles with radiating spokes (color figure online)

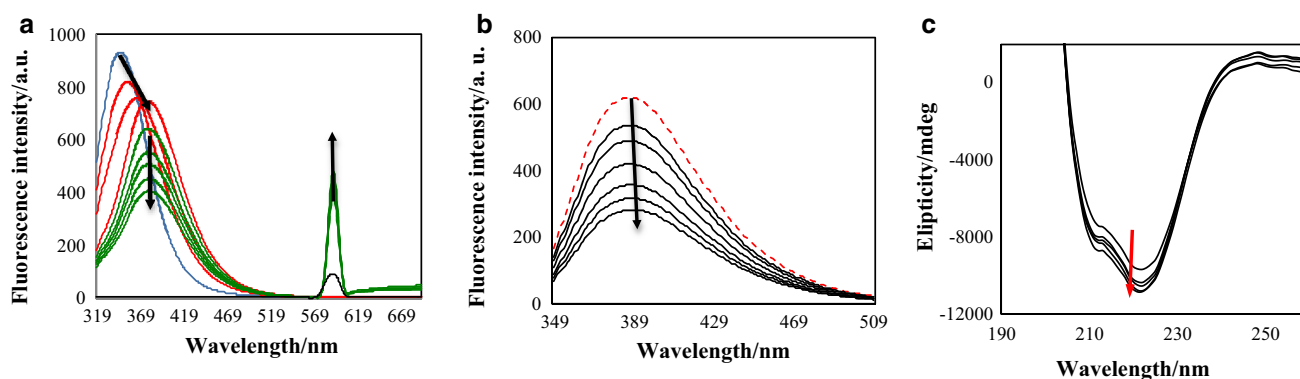


Fig. 6 Fluorescence spectra of HSA, warfarin:HSA binary mixture and warfarin:HSA:α-LA ternary mixture in phosphate buffer of pH 7.4 at 298 K ($\lambda_{\text{ex}}=295$ nm). Blue curve shows HSA at the concentration of 1.5 μM , red curves show the HSA–warfarin binary mixture in the molar ratio of $[\text{WAR}]/[\text{HSA}]=0.34, 0.68,$ and 1.02 and green curves show the warfarin–HSA–α-LA ternary mixture in the molar ratio of $[\text{warfarin}]:[\text{HSA}]:[\alpha\text{-LA}]=1.02:1.5:0.06, 1.02:1.5:1.27, 1.02:1.5:1.90,$ and $1.02:1.5:2.54$. Black curve shows α-LA at the concentration of 1.96×10^{-5} M in phosphate buffer pH 7.4 (a). Fluorescence spectra of the warfarin:HSA binary mixture

and warfarin:HSA:α-LA ternary mixture in phosphate buffer of pH 7.4 at 298 K ($\lambda_{\text{ex}}=330$ nm). Red curve shows the HSA–warfarin binary mixture in the molar ratio of $[\text{warfarin}]/[\text{HSA}]=1.02$, black curves show the α-LA:HSA:warfarin ternary mixture in the molar ratio of $[\text{warfarin}]:[\text{HSA}]:[\alpha\text{-LA}]=1.02:1.5:0.06, 1.02:1.5:1.27, 1.02:1.5:1.90,$ and $1.02:1.5:2.54$ (b). Far-UV CD spectra of HSA in the presence of various concentrations of α-LA (0, 0.49, 0.99, 2.4, 4.9, 7.3, 9.8×10^{-6} M) at pH 7.4 and environment temperature (c) (color figure online)

Alteration in HSA conformation

CD spectra in the far-UV region were used to follow conformational changes in the secondary structure of HSA during gradual addition of α-LA in the system. The spectra are shown in Fig. 6c. The α-helical structure of HSA is characterized by two minima at 208 and 222 nm in the far-UV region of the spectra. The binding of α-LA to HSA caused a rise in the band intensity at all wavelengths of the far-UV CD while keeping the positions of the peaks. This clearly indicates that the secondary structure of HSA is changing in the direction of increasing helicity. According to the results analyzed by the CDNN software, the α-helical content of HSA grew from 51.12% in the absence of α-LA to 63% at highest concentration of α-LA. Such an increase was also observed with gradual addition of tolperisone hydrochloride to HSA solution [48]. Additionally, a 7% decline in random coil content of HSA from 22.8 to 15.7% proved a more ordered structure of HSA, in the presence of α-LA. These data are in good accordance with the results respective to molecular dynamics in the previous section. Note that the greatest conformational modifications were observed at high concentrations of α-LA.

Thermal stability of the complex

To investigate the impact of α-LA on the thermal stability of HSA, emission spectra of HSA and its complex with α-LA were recorded within the temperature range of 293–373 K. Heating was accompanied by diminished fluorescence intensity of HSA and the unexpected shift of the emission

maximum wavelength to shorter wavelengths which were up to 13 and 14 nm for HSA and the HSA–α-LA complex, respectively. Such a blue shift can be explained when Trp is located in a more hydrophobic environment in response to conformational alterations induced by the protein unfolding [49, 50]. Borzova et al. attributed a similar blue shift in bovine serum albumin to dimerization of unfolded monomers followed by localization of Trp residues in more hydrophobic surroundings [51]. Heat denaturation of HSA and HSA–α-LA complex was monitored based on changes in the fluorescence intensity at a maximum wavelength of 340 nm. Figure 7a reveals heat induced denaturation curves of HSA in the presence and absence of α-LA, both assumed to have a typical two-state denaturation behavior (native \rightleftharpoons denatured). Transition curves were analyzed to obtain the transition temperature (T_m) and heat of denaturation (ΔH_D) through a non-linear least-square analysis according to the following equation [52]:

$$Y_{\text{obs}} = \frac{Y_N(T) + Y_D(T) \exp[(\Delta H_D/R)(1/T - 1/T_m)]}{1 + \exp[(\Delta H_D/R)(1/T - 1/T_m)]}, \quad (6)$$

where Y_{obs} is the observed fluorescence intensity at maximum wavelengths of 342 and 339 nm, for HSA and its complex, respectively. $Y_N(T)$ and $Y_D(T)$ represent the intensity of the native and denatured proteins at the absolute temperature T . The linear equations corresponding to Y_N and Y_D are shown in Fig. 7a.

As reported in Table 2, the positive values of ΔH_D and ΔG_{25}° indicate that denaturation process of HSA is endothermic and non-spontaneous. The rise in the transition

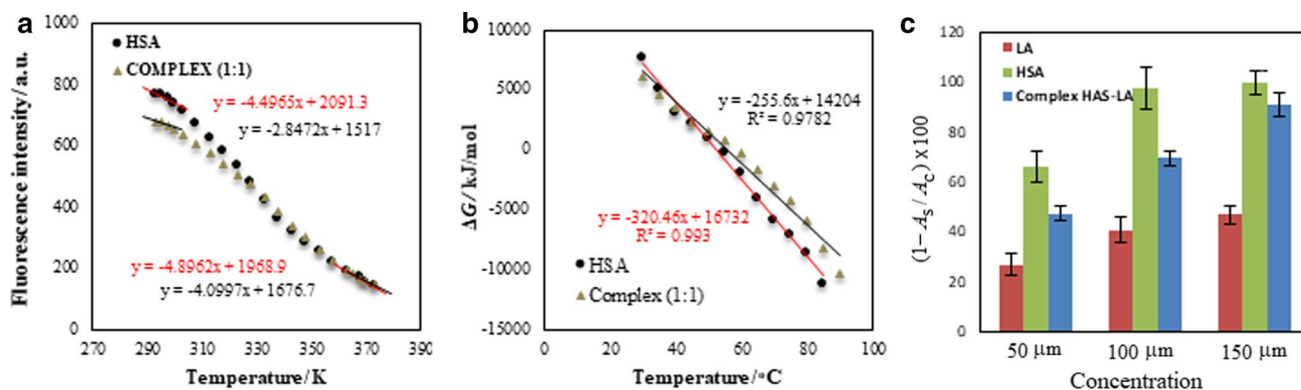


Fig. 7 Unfolding profile of HSA (3 mM) and its complex with α -LA dissolved in 10 mM phosphate buffer pH 7.4, the plot is obtained from plotting protein fluorescence as a function of temperature (a).

Standard Gibbs energy of unfolding plots in the absence and presence of α -LA (b). Antioxidant activity of α -LA/HSA/HSA- α -LA complex at 50, 100, 150 μ M determined by the ABTS radical scavenging (c)

Table 2 Transition temperature and thermodynamic parameters of HSA denaturation in the absence and presence of α -LA

Sample	T_m /K	ΔG_{25}° /kJ mol $^{-1}$	ΔH_D /kJ mol $^{-1}$
HSA	340.15 \pm 273.70	8.72 \pm 0.09	97.67 \pm 1.82
Complex of HSA- α -LA (1:1)	345.82 \pm 274.08	7.81 \pm 0.10	120.10 \pm 1.99

temperature and enthalpy of denaturation were the most notable findings of this study. The change in T_m from 67.2 to 72.8 $^\circ$ C was accompanied by about 22 kJ/mol growth in the ΔH_D value (Table 2). The effect of α -LA on the folding of HSA in the subdomain IIA was revealed by an obvious blue shift during the titration (Fig. 1a), which can be the probable reason for the increasing changes of denaturation parameters of HSA associated with α -LA. On the other hand, the blue shift observed during heating cannot be effective on denaturation parameters, since it occurred for both free HSA and its complex with α -LA. In addition, the increased thermostability due to the interaction with α -LA is probably related to the coupling between the protein denaturation and ligand-binding equilibria [53].

To estimate the conformational stability of HSA at room temperature, the transition curves were used to estimate the denatured fraction of protein according to the following equation [54]:

$$f_d = \frac{Y_N - Y_{\text{obs}}}{Y_N - Y_D}, \quad (7)$$

where Y_{obs} , Y_N , and Y_D were determined at each point of the transition region. Considering the two-state theory of denaturation, the change in standard Gibbs free energy (ΔG_{25}°) value for HSA denaturation at different temperatures can be

calculated through the equilibrium constant (K_D) value of denaturation, according to Eqs. (8) and (9):

$$K_D = \frac{f_d}{1 - f_d}, \quad (8)$$

$$\Delta G^\circ = -RT \ln K_D. \quad (9)$$

The HSA stability was estimated through continuing the linear dependence of ΔG° to 25 $^\circ$ C (Fig. 7b). The diminished stability of HSA in the presence of α -LA appeared as a drop in the ΔG_{25}° value of HSA from 8.7 to 7.8 kJ/mol (Table 2). Since the results in Fig. 1a indicate partial folding of HSA bound to α -LA and subsequently greater contribution of stabilizing forces to native HSA structure, the lowered stability of HSA can be explained based on its increased conformational entropy in comparison with the free protein.

ABTS radical scavenging activity

The blue-green ABTS $^{+\cdot}$ radical generated by the reaction between ammonium persulfate and ABTS can be reduced by the electron donated from an antioxidant, thereby leading to a loss of absorbance at 734 nm [55]. The results revealed that HSA had the highest activity to scavenge ABTS $^{+\cdot}$ radical (Fig. 7c). Part of the unique antioxidant property of HSA is due to its free radical-trapping ability through its residues. The two groups of sulfur-containing residues including Cys34 and 6 methionine residues are oxidation-sensitive amino acids contributing to the antioxidant activity of HSA against free radicals [56]. α -LA is unique amongst biological antioxidants and due to its advantage of possessing a special sulfur-containing structure, it can scavenge various types of free radicals [2].

As can be seen in Fig. 7c, the antioxidant activity of α -LA was enhanced when combined with HSA, but it was

less than that of free HSA. Indeed, it can be suggested that the antioxidant capacity of HSA is, therefore, masked by its interaction with α -LA. This could be justified based on involvement of two different types of antioxidant residues of HSA with α -LA; these residues could lie in a position no longer accessible to the free radicals following conformational changes of HSA induced by α -LA binding [17]. Nevertheless, the radical scavenging activities increased for all three species of HSA, α -LA, and their complex, as the concentration increased from 50 to 150 μ M.

Photostability of the HSA- α -LA complex

A distorted five-membered 1,2-dithiolane structure makes α -LA susceptible to light irradiation, thus leading to the deterioration of its representative absorption peak at 330 nm. To investigate the role of HSA in the protection of α -LA against UV light (UVA, UVB, and UVC), the absorbance at the mentioned wavelength was followed at given time intervals. As can be seen in Fig. 8a, the characteristic band of α -LA solution irradiated with long-wavelength UV (UVA and UVB) diminished with increasing exposure time.

The reduced absorbance is probably due to the rupture of disulfide (S-S) bond accompanied by an increment in the concentration of thiol groups [56]. Further, the degradation of α -LA has been combined with the simultaneous generation of DHLA (dihydrolipoic acid), which would form through intra- or intermolecular hydrogen atom abstraction of dithiyl radicals [57]. It can be seen from Fig. 8b that HSA protects α -LA from photodecomposition irradiated with long wavelengths of UV, such that its absorption spectra remained unchanged during the irradiation time. On the other hand, α -LA degraded at a rate constant of 0.003 min^{-1} by assuming first-order kinetics for its photodecomposition (Fig. 8c). Thiol compounds result in improved recovery of α -LA through inducing DHLA generation. Thiol groups in methionine and cysteine residues of HSA can contribute to the protective effect of HSA on α -LA. In addition to the antioxidant role of HSA in scavenging dithiyl radicals, presumably preventing the production of reactive oxygen species (ROS), it would be able to inactivate ROS [58]. The increase of absorption at wavelengths $< 280 \text{ nm}$ (Fig. 8a) could be ascribed to the formation of linear disulfide polymers, followed by the S-S bond cleavage [59].

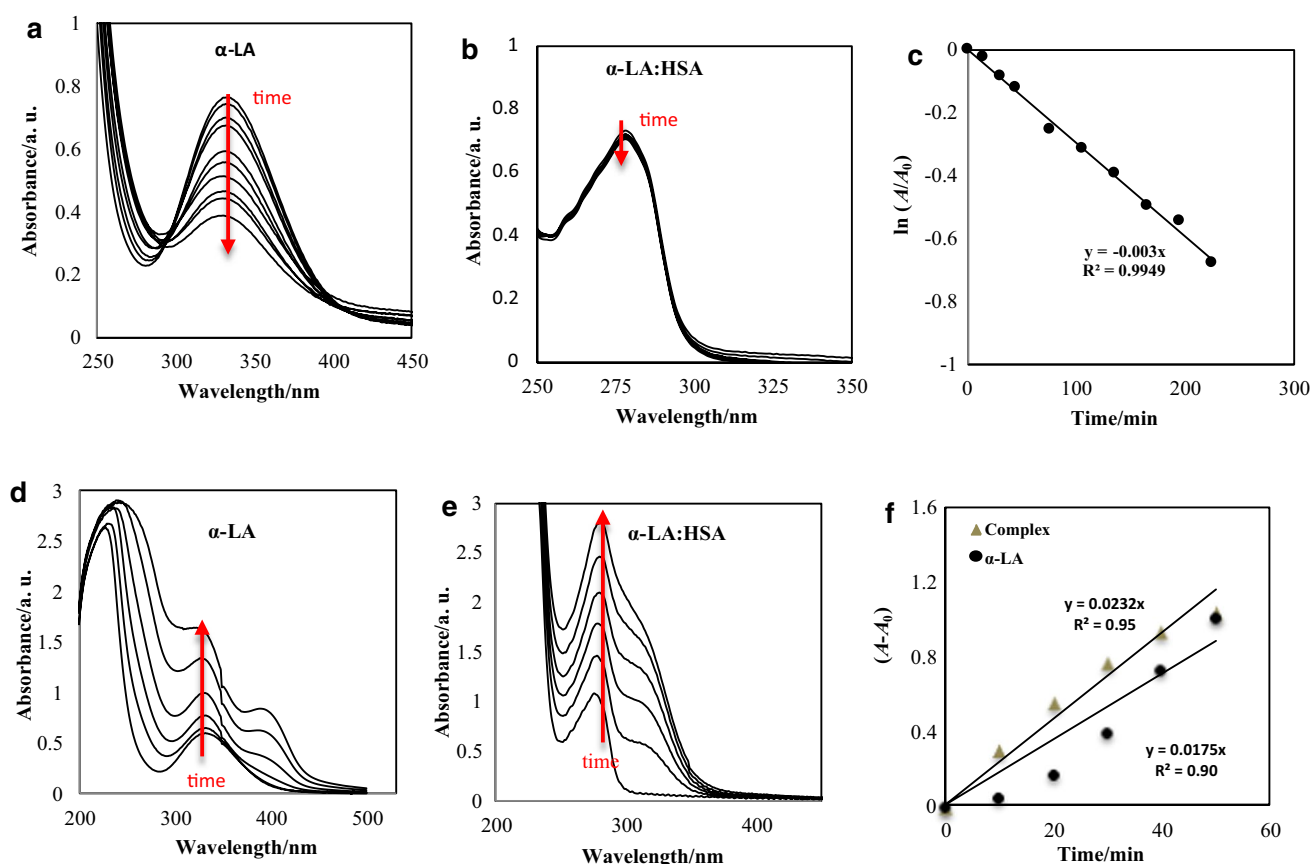


Fig. 8 Spectral changes of α -LA (a) and HSA- α -LA complex (b) under UVA and UVB radiation and the degradation kinetics curve of α -LA under UVA and UVB radiation (c). Spectral changes of α -LA

(d) and HSA- α -LA complex (e) under UVC radiation and their degradation kinetics curves under UVC radiation (f)

Unexpectedly, UVC irradiation increased the absorption band of 330 nm (Fig. 8d), which can be attributed to the rebuilding of α -LA from its photoproducts [59]. The photoionization process of α -LA and DHLA under short-wavelength UV irradiation generates cation radicals (LA^+) and anion radicals (LA^-). Finally, equimolar amounts of α -LA and DHLA are produced from the latter. The emergence of a new band at about 400 nm is related to the generated radical species [59]. Although the peak respective to α -LA associated with HSA shifted to shorter wavelengths, it underwent the same increment (Fig. 8e).

The degradation kinetics of α -LA in complexation with HSA under UVC irradiation was followed the zero-order model as shown in Eq. (10). Although the adequacy of first-order model is better than that of zero-order for photodegradation kinetics of α -LA, we applied the zero-order one to compare the degradation rate of the two samples:

$$A - A_0 = -kt, \quad (10)$$

where A is the absorbance of α -LA at a given time, A_0 denotes the initial absorbance of α -LA, k is the rate constant, and t represents the treatment time. The rate constant of photodegradation in the UVC region for the free and complexed form of α -LA is $0.017 \text{ min}^{-1} \text{ M}$ and $0.023 \text{ min}^{-1} \text{ M}$, respectively (Fig. 8f). The higher rate of α -LA regeneration in the presence of HSA confirms its protective activity.

Conclusion

Taken together, this study proved that α -LA and HSA form a complex with a binding stoichiometry of 1:1 (α -LA: HSA). Both *in silico* and *in vitro* data confirmed that hydrogen bond and van der Waals interactions are the main forces in stabilizing the resulting complex. Both of CD and DSSP analysis showed an increment in α -helix and a decrement in random coils structures. The enhanced thermal stability of the protein, notable improvement in the stability of α -LA against UV irradiations, and its greater ability in scavenging free radicals are among outcomes of the association process between α -LA and HSA. The findings of this research can be helpful in the food and pharmaceutical industries to apply HSA as an efficient delivery system for α -LA.

Experimental

HSA fraction V (fatty acid free, 99%) and a racemic mixture of α -LA were purchased from Sigma Chemical Company (St. Louis, MO, USA). Phosphate salts and absolute ethanol were purchased from Merck (Darmstadt, Germany). α -LA was dissolved in ethanol at concentration of 7.7 mM as a

stock solution and then diluted by phosphate buffer (10 mM) to 0.5 mM.

Fluorescence studies

The fluorescence spectra were recorded using a Carry Eclipse (Varian, Australia) spectrofluorometer. The excitation wavelength was set at 295 nm for all measurements. Both excitation and emission slits were set to 5 nm. The emission spectra were recorded between 290 and 450 nm at two temperatures (298 and 310 K). Further, 1 cm^3 of HSA solution (3 μM) prepared in 10 mM phosphate buffer (pH 7.4) was titrated with 2 mm^3 -aliquots of the diluted solution of α -LA (0.5 mM). The total amount of ethanol added to the system did not exceed 0.2% of the total volume at the end of titration [60, 61].

Circular dichroism (CD) spectroscopy

CD spectroscopy was conducted using a spectropolarimeter (Aviv, 215, USA) in the far-UV region (200–250 nm), at 25 °C. The concentrations used were similar to those in the fluorescence studies. Far-UV CD spectra were recorded at the protein concentration of 3 μM in the absence and presence of 0.49, 0.99, 2.4, 4.9, 7.3, and 9.8 μM concentrations of α -LA. Note that the signal of α -LA was subtracted from signals corresponding to the HSA combined with α -LA.

The obtained data were converted to molar ellipticity, $[\theta]$ ($\text{deg cm}^2 \text{ dmol}^{-1}$), by the CDNN software according to Eq. (11) [61–64], as follows:

$$[\theta] = \frac{\theta}{R \times c \times l \times 10}, \quad (11)$$

where θ is the CD signal in degree at each wavelength, c denotes the protein concentration in mol/cm^3 , l represents the length of light path (cm), and R is residue number of HSA. The elements constituting up protein secondary structure were determined using a statistical method through the CDNN software [62].

Binding stoichiometry

Job's method was applied to determine the binding stoichiometry of the resulting complex [65]. According to this method, by keeping the total concentration [α -LA + HSA] constant, the molar fractions of α -LA and HSA were changed. Two solutions of α -LA and HSA with similar concentrations (3 μM) were mixed at different ratios. The total volume of the mixed solutions was kept constant and consequently the total moles of reactants in each mixture were constant. A measurable parameter proportional to the complex concentration was plotted vs. the HSA molar fraction, according to Eq. (12) [63]:

$$[C] = (F_0 - F) \times [P], \quad (12)$$

where $[P]$ represents the molar fraction of protein and F_0 and F are proportional to the total HSA and unbound (free) HSA concentration, respectively. The binding stoichiometry of the complex was determined from the position of the maximum appearing on the plot [65].

Thermal stability of the complex

A solution containing equimolar concentrations of α -LA and HSA (10 μ M) was prepared. After 5 min of timing, emission spectra of HSA at excitation wavelength of 295 nm were recorded within the temperature range of 293 to 373 K. The same experiment was done for HSA alone [61].

Molecular docking

To investigate the preferential binding site of α -LA in HSA and the mode of interaction between the α -LA and HSA molecules, molecular docking was performed by the AutoDock Vina 1.1.2 program [66]. AutoDock Tools 1.5.6 [67] was used to prepare the PDBQT input files for the protein and ligand by assigning the charges of HSA residues using Kollman charges [68] and adding Gasteiger charges [69] to the α -LA. All other docking parameters were set to their default values. The chemical structure of α -LA was obtained from ZINC database (ZINC ID: 1532729). Coordinates of the HSA were acquired from the PDB code, 1AO6. Initially, all crystal water molecules were removed from the PDB file. The reduce software (<http://kinemage.biochem.duke.edu/software/reduce.php>) was applied to add hydrogen atoms to HAS [70–72].

Molecular dynamics simulation

To validate the obtained docking results and to evaluate the effect of α -LA on the HSA structure, two molecular dynamics (MD) simulations were applied (free HSA, HSA— α -LA complex). The Antechamber module from the Amber Tools 14 [73] suite was used to obtain the topology of α -LA molecule with the GAFF force field [74], while Amber 03 force field [75] was considered for HSA molecule. AM1-BCC charges were assigned to the α -LA molecule. All MD simulations were carried out using the GROMACS package [76], version 5.1.3 through the leapfrog algorithm with a time step of 2 fs. Each system was placed in a periodic box with a closeness parameter of 10 Å. The boxes were then filled with appropriate amounts of TIP3P water molecules. The fifteen Na^+ counter ions were added to maintain the electro-neutrality of the systems. Further, the particle mesh Ewald (PME) method [77] was used to treat the long-range electrostatic interactions. The SHAKE algorithm [78] was

used to constrain all bonds involving hydrogen atoms. Further, the initial velocities were taken from a Maxwell–Boltzmann distribution at 300 K. The cutoff distance for van der Waals interactions was set to 10 Å. The constant temperature (300 K) and pressure (1 bar) were obtained by applying the Nose–Hoover thermostat [79, 80] and Parrinello–Rahman barostat [81], respectively. The time constants used for coupling the barostat and thermostat to the system were 2.0 and 0.1 ps, respectively. The value of the isothermal compressibility was set to $4.5 \times 10^{-5} \text{ bar}^{-1}$. All systems were energy minimized by the steepest descent method with position restraints of $1000 \text{ kJ mol}^{-1} \text{ nm}^{-2}$ on all heavy atoms to remove unsuitable contacts. This was followed by two equilibration phases in the NVT and NPT ensembles with position restraints to relax the system. Lastly, a production phase was performed for 50 ns under an NPT ensemble. The atomic coordinates were saved every 5 ps for analysis. PyMOL (The PyMOL Molecular Graphics System, Version 1.2r3pre, Schrödinger, LLC.) was used to visualize the docked conformations and to create the molecular graphic images.

Site-competitive experiments

Site-competitive experiments were performed using warfarin as a Sudlow I site marker. To this aim, after warfarin addition to the HSA solution, the titration continued with gradual addition of α -LA. Two excitation wavelengths of 295 and 330 nm were used to investigate the competition between two ligands. All experiments of this part were performed at 298 K [82].

Complex preparation

Stock solution of α -LA was prepared freshly with the concentration of 7.7 mM in ethanol followed by dilution to a specific concentration using 10 mM phosphate buffer. Complex samples for the following experiments were prepared by the drop-by-drop addition of diluted stock solution of α -LA to the protein solutions under magnetic stirring to finally achieve the molar ratio of interest.

Photostability of α -LA

To investigate the light endurance of α -LA in complexation with HSA, the samples were irradiated at two wavelength ranges at room temperature and pressure. The solutions of α -LA and their complexes in quartz cuvettes with a path length of 1 cm were illuminated by two UVC lamps (Philips Sterilamp G8T5) and a UVA–UVB lamp (Narva LT18W). Absorption of samples were measured every 15 min over 225 min. Absorption spectra of α -LA and their complexes were collected using a spectrometer (Cary 100 Conc.,

Australia) within the wavelength range of 190–600 nm. Quartz cuvettes with a path length of 1 cm were used to record the absorption spectra.

ABTS^{•+} radical scavenging activity

ABTS^{•+} radical cation scavenging activity was determined according to the method presented previously [83]. The cation radical of ABTS^{•+} was prepared by mixing 7 mM ABTS stock solution with 2.45 mM potassium persulfate (at a final concentration). The resulting solution was stored in the dark at an ambient temperature for 14–16 h. The radical solution was diluted using 95% ethanol with its absorbance adjusted to 0.7 at 734 nm prior to use. Further, 700 mm³ of ABTS^{•+} was added to 300 mm³ of sample and the reaction mixture was allowed to stand at room temperature for 6 min with the absorbance immediately read at 734 nm [84]. The scavenging activity was estimated using the following equation:

$$\text{Scavenging\%} = \frac{(A_{\text{sample}} - A_{\text{blank}})}{A_{\text{blank}}}, \quad (13)$$

where A_{blank} is absorbance of the blank sample ($t = 0$).

Supplementary Information The online version contains supplementary material available at <https://doi.org/10.1007/s00706-021-02858-9>.

Acknowledgements This work was financially supported by University of Tehran. We would like to thank Fatemeh Fatemi-Nasab for her advice in some tests done in this research.

References

- Packer L, Witt EH, Tritschler HJ (1995) *Free Radic Biol Med* 19:227
- Data P (1995) *Arzneimittelforsch* 45:872
- Goraça A, Huk-Kolega H, Piechota A, Kleniewska P, Ciejka E, Skibska B (2011) *Pharmacol Rep* 63:849
- Holmquist L, Stuchbury G, Berbaum K, Muscat S, Young S, Hager K, Münch G (2007) *Pharmacol Ther* 113:154
- Maczurek A, Hager K, Kenkies M, Sharman M, Martins R, Engel J, Münch G (2008) *Adv Drug Deliv Rev* 60:1463
- Shay KP, Moreau RF, Smith EJ, Smith AR, Hagen TM (2009) *Biochim Biophys Acta Gen Subj* 1790:1149
- Li Y, Zhao Y, Yu W, Jiang S (2004) *Food Chem* 84:563
- Beitner H (2003) *Br J Dermatol* 149:841
- Atukeren P, Aydin S, Uslu E, Gumustas M, Cakatay U (2010) *Oxid Med Cell Longev* 3:206
- Packer L, Cadenas E (2010) *J Clin Biochem Nutr* 48:26
- Akkas SB, Severcan M, Yilmaz O, Severcan F (2007) *Food Chem* 105:1281
- Wada N, Wakami H, Konishi T, Matsugo S (2009) *J Clin Biochem Nutr* 44:218
- Wang J, Tang J, Zhou X, Xia Q (2014) *Drug Dev Ind Pharm* 40:201
- Teichert J, Hermann R, Ruus P, Preiss R (2003) *J Clin Pharmacol* 43:1257
- Kofuji K, Nakamura M, Isobe T, Murata Y, Kawashima S (2008) *Food Chem* 109:167
- Zheng M, Tang W, Kong R, Zhu X (2017) *Indian J Pharm Sci* 79:544
- Ikuta N, Sugiyama H, Shimosegawa H, Nakane R, Ishida Y, Uekaji Y, Matsugo S (2013) *Int J Mol Sci* 14:3639
- Takahashi H, Bungo Y, Mikuni K (2011) *Biosci Biotechnol Biochem* 75:633
- Lasoń E, Sikora E, Miastkowska M, Socha P, Ogonowski J (2017) *Colloids Surf A Physicochem Eng Asp* 532:57
- Li YX, Park EY, Lim ST (2018) *Food Chem* 242:389
- Suji G, Khedkar SA, Singh SK, Kishore N, Coutinho EC, Bhor VM, Sivakami S (2008) *Protein J* 27:205
- Wang W, Huang Y, Zhao S, Shao T, Cheng Y (2013) *Chem Commun (Camb)* 49:2234
- Rabbani G, Baig MH, Lee EJ, Cho WK, Ma JY, Choi I (2017) *Mol Pharm* 14:1656
- Fanali G, Masi AD, Trezza V, Marino M, Fasano M, Ascenzi P (2012) *Mol Aspects Med* 33:209
- Rabbani G, Ahn SN (2019) *Int J Biol Macromol* 123:979
- Al-Harathi S, Lachowicz JI, Nowakowski ME, Jaremko M, Jaremko Ł (2019) *J Inorg Biochem* 198:110716
- Cuya Guizado IR, Louro SRW, Anteneodo C (2012) *Eur Biophys J* 41:1031
- Karami L, Saboury AA, Rezaee E, Tabatabai SA (2017) *Eur Biophys J* 46:445
- Varlan A, Hillebrand M (2010) *Molecules* 15:3905
- Zhang Y, Zhong Q (2012) *J Agric Food Chem* 60:1880
- Afrin S, Rabbani G, Khan RH (2014) *J Lumin* 151:219
- Khan S, Ahmad R, Naseem I (2021) *J Biomol Struct Dyn* 39:970
- Ghosh N, Mondal R, Mukherjee S (2015) *Langmuir* 31:8074
- Tian FF, Jiang FL, Han XL, Xiang C, Ge YS, Li JH, Liu Y (2010) *J Phys Chem B* 114:14842
- Barik A, Mishra B, Kunwar A, Priyadarsini KI (2007) *Chem Phys Lett* 436:239
- Fredrickson DS, Gordon RS Jr (1958) *Physiol Rev* 38:585
- Fredrickson DS, Gordon RS (1958) *J Clin Invest* 37:1504
- Zhang Y, Zhong Q (2013) *Food Chem* 139:611
- Geethanjali HS, Nagaraja D, Melavanki RM, Kusanur RA (2015) *J Lumin* 167:216
- Ross PD, Subramanian S (1981) *Biochemistry* 20:3096
- Shamsi A, Al Shahwan M, Ahamad S, Hassan MI, Ahmad F, Islam A (2020) *J Biomol Struct Dyn* 38:1094
- Rabbani G, Ahmad E, Zaidi N, Fatima S, Khan RH (2012) *Cell Biochem Biophys* 62:487
- Allahdad Z, Varidi M, Zadmand R, Saboury AA, Haertlé T (2019) *Food Chem* 277:96
- Kabsch W, Sander C (1983) *Biopolymers* 22:2577
- Wallace AC, Laskowski RA, Thornton JM (1995) *Protein Eng Des Sel* 8:127
- Petitpas I, Bhattacharya AA, Twine S, East M, Curry S (2001) *J Biol Chem* 276:22804
- Sudlow GDJB, Birkett DJ, Wade DN (1975) *Mol Pharmacol* 11:824
- Rabbani G, Lee EJ, Ahmad K, Baig MH, Choi I (2018) *Mol Pharm* 15:1445
- Rabbani G, Ahmad E, Zaidi N, Khan RH (2011) *Cell Biochem Biophys* 6:551
- Rabbani G, Ahmad E, Khan MV, Ashraf MT, Bhat R, Khan RH (2015) *RSC Adv* 5:20115
- Borzova VA, Markossian KA, Chebotareva NA, Kleymenov SY, Poliansky NB, Muranov KO, Kurganov BI (2016) *PLoS ONE* 11:e0153495
- Rahman S, Ali SA, Islam A, Hassan MI, Ahmad F (2016) *Arch Biochem Biophys* 591:7
- Celej MS, Montich GG, Fidelio GD (2003) *Protein Sci* 12:1496

54. Saboury AA, Moosavi-Movahedi AA (1995) *Biochem Educ* 23:164
55. Luo Y, Pan K, Zhong Q (2014) *Food Chem* 155:46
56. Taverna M, Marie AL, Mira JP, Guidet B (2013) *Ann Intensive Care* 3:4
57. Matsugo S, Han D, Tritschler HJ, Packer L (1996) *Biochem Mol Biol Int* 38:51
58. Elias RJ, Kellerby SS, Decker EA (2008) *Crit Rev Food Sci Nutr* 48:430
59. Bucher G, Lu C, Sander W (2005) *ChemPhysChem* 6:2607
60. Rahman Y, Afrin S, Alhaji Isa M, Ahmed S, Tabish M (2020) *J Biomol Struct Dyn* 38:1375
61. Delavari B, Saboury AA, Atri MS, Ghasemi A, Bigdeli B, Khammari A, Goliaei B (2015) *Food Hydrocoll* 45:124
62. Böhm G, Muhr R, Jaenicke R (1992) *Des Select* 5:191
63. Allahdad Z, Varidi M, Zadmand R, Saboury AA (2018) *Food Chem* 255:187
64. Sun X, Bi S, Wu J, Zhao R, Shao D, Song Z (2020) *J Biomol Struct Dyn* 38:934
65. Huang CY (1982) *Methods Enzymol* 87:509
66. Trott O, Olson AJ (2010) *Comput Chem* 31:455
67. Sanner MF (1999) *J Mol Graph Model* 17:57
68. Weiner SJ, Kollman PA, Case DA, Singh UC, Ghio C, Alagona G, Weiner P (1984) *J Am Chem Soc* 106:765
69. Gasteiger J, Marsili M (1980) *Tetrahedron* 36:3219
70. Ahmad E, Rabbani G, Zaidi N, Singh S, Rehan M, Khan MM, Subbarao N (2011) *PLoS ONE* 6:e26186
71. Varshney A, Rehan M, Subbarao N, Rabbani G, Khan RH (2011) *PLoS ONE* 6:e17230
72. Ahmad E, Rabbani G, Zaidi N, Ahmad B, Khan RH (2012) *PLoS ONE* 7:e38372
73. Pearlman DA, Case DA, Caldwell JW, Ross WS, Cheatham TE III, DeBolt S, Kollman P (1995) *Comput Phys Commun* 91:1
74. Wang J, Wolf RM, Caldwell JW, Kollman PA, Case DA (2004) *J Comput Chem* 25:1157
75. Duan Y, Wu C, Chowdhury S, Lee MC, Xiong G, Zhang W, Yang R, Cieplak P, Luo R, Lee T, Caldwell J, Wang J, Kollman P (2003) *J Comput Chem* 24:1999
76. Spoel VD, Lindahl E, Hess B, Groenhof G, Mark AE, Berendsen HJ (2005) *J Comput Chem* 26:1701
77. Essmann U, Perera L, Berkowitz ML, Darden T, Lee H, Pedersen LG (1995) *J Chem Phys* 103:8577
78. Ryckaert J-P, Ciccotti G, Berendsen HJC (1977) *J Comput Phys* 23:327
79. Nose S (1984) *J Chem Phys* 81:511
80. Hoover WG (1985) *Phys Rev A* 31:1695
81. Parrinello M, Rahman A (1981) *J Appl Phys* 52:7182
82. Khammari A, Saboury AA, Karimi-Jafari MH, Khoobi M, Ghasemi A, Yousefinejad S, Abou-Zied OK (2017) *J Chem Phys* 19:10099
83. Re R, Pellegrini N, Proteggente A, Pannala A, Yang M, Rice-Evans C (1999) *Free Radic Biol Med* 26:1231
84. Ishtikhar M, Rabbani G, Khan S, Khan RH (2015) *RSC Adv* 5:18218

Publisher's Note Springer Nature remains neutral with regard to jurisdictional claims in published maps and institutional affiliations.